Atmos. Chem. Phys., 11, 10837–10851, 2011
www.atmos-chem-phys.net/11/10837/2011/
doi:10.5194/acp-11-10837-2011


Atmospheric Chemistry and Physics

# Rate coefficients for the reaction of methylglyoxal ($CH_3COCHO$) with OH and $NO_3$ and glyoxal $(HCO)_2$ with $NO_3$

**R. K. Talukdar[1,2], L. Zhu[1,2], K. J. Feierabend[1,2], and J. B. Burkholder[1]**

[1]Chemical Sciences Division, Earth System Research Laboratory, NOAA 325 Broadway, Boulder, CO 80305-3328, USA
[2]Cooperative Institute for Research in Environmental Sciences, University of Colorado, Boulder, CO 80309, USA

Received: 3 June 2011 – Published in Atmos. Chem. Phys. Discuss.: 27 June 2011
Revised: 20 September 2011 – Accepted: 17 October 2011 – Published: 2 November 2011

**Abstract.** Rate coefficients, $k$, for the gas-phase reaction of $CH_3COCHO$ (methylglyoxal) with the OH and $NO_3$ radicals and $(CHO)_2$ (glyoxal) with the $NO_3$ radical are reported. Rate coefficients for the $OH + CH_3COCHO$ ($k_1$) reaction were measured under pseudo-first-order conditions in OH as a function of temperature (211–373 K) and pressure (100–220 Torr, He and $N_2$ bath gases) using pulsed laser photolysis to produce OH radicals and laser induced fluorescence to measure its temporal profile. $k_1$ was found to be independent of the bath gas pressure with $k_1(295\,\mathrm{K}) = (1.29 \pm 0.13) \times 10^{-11}$ cm$^3$ molecule$^{-1}$ s$^{-1}$ and a temperature dependence that is well represented by the Arrhenius expression $k_1(T) = (1.74 \pm 0.20) \times 10^{-12}$ exp$[(590 \pm 40)/T]$ cm$^3$ molecule$^{-1}$ s$^{-1}$ where the uncertainties are $2\sigma$ and include estimated systematic errors. Rate coefficients for the $NO_3$ + $(CHO)_2$ ($k_3$) and $NO_3 + CH_3COCHO$ ($k_4$) reactions were measured using a relative rate technique to be $k_3(296\,\mathrm{K}) = (4.0 \pm 1.0) \times 10^{-16}$ cm$^3$ molecule$^{-1}$ s$^{-1}$ and $k_4(296\,\mathrm{K}) = (5.1 \pm 2.1) \times 10^{-16}$ cm$^3$ molecule$^{-1}$ s$^{-1}$. $k_3(T)$ was also measured using an absolute rate coefficient method under pseudo-first-order conditions at 296 and 353 K to be $(4.2 \pm 0.8) \times 10^{-16}$ and $(7.9 \pm 3.6) \times 10^{-16}$ cm$^3$ molecule$^{-1}$ s$^{-1}$, respectively, in agreement with the relative rate result obtained at room temperature. The atmospheric implications of the OH and $NO_3$ reaction rate coefficients measured in this work are discussed.

*Correspondence to:* R. K. Talukdar
(ranajit.k.talukdar@noaa.gov)

## 1 Introduction

Methylglyoxal, $CH_3COCHO$, and glyoxal, $(HCO)_2$, are dicarbonyls that play an important role in atmospheric chemistry as tracers of atmospheric biogenic and anthropogenic organic chemistry. They also play a role in tropospheric ozone production and secondary organic aerosol (SOA) formation on local to regional scales (Ervens and Volkamer, 2010). Methylglyoxal and glyoxal are short-lived species that are removed from the atmosphere primarily by UV/visible photolysis, gas-phase reaction, and heterogeneous processes. Studies of the OH radical reaction with glyoxal and its UV/visible photolysis quantum yields have been reported in previous work from this laboratory (Feierabend et al., 2008, 2009). In this work, rate coefficients for the OH radical reaction with methylglyoxal and the $NO_3$ radical reaction with glyoxal and methylglyoxal are presented.

Methylglyoxal is formed in the degradation of volatile organic compounds including isoprene and the aromatic hydrocarbons toluene, xylene, and trimethylbenzene. Methylglyoxal is also emitted directly into the atmosphere via the incomplete combustion of fossil fuels and biomass and to a lesser extent in automobile emissions as a result of biofuel usage. Approximately 30 % of the atmospheric oxidation of isoprene, the biogenic hydrocarbon with the greatest global emission, leads to the formation of methylglyoxal (Paulot et al., 2009; Paulson and Seinfeld, 1992), which accounts for ∼79 % of the methylglyoxal atmospheric budget. The atmospheric degradation of acetone is the next largest source of methylglyoxal and accounts for ∼7 % of its budget (Fu et al., 2008). The atmospheric abundance of methylglyoxal varies depending on location and season with gas-phase values of ∼0.15 ppb and particle-phase concentrations in the range 0.1–8.0 ng m$^{-3}$ reported in urban and rural areas (Grossmann

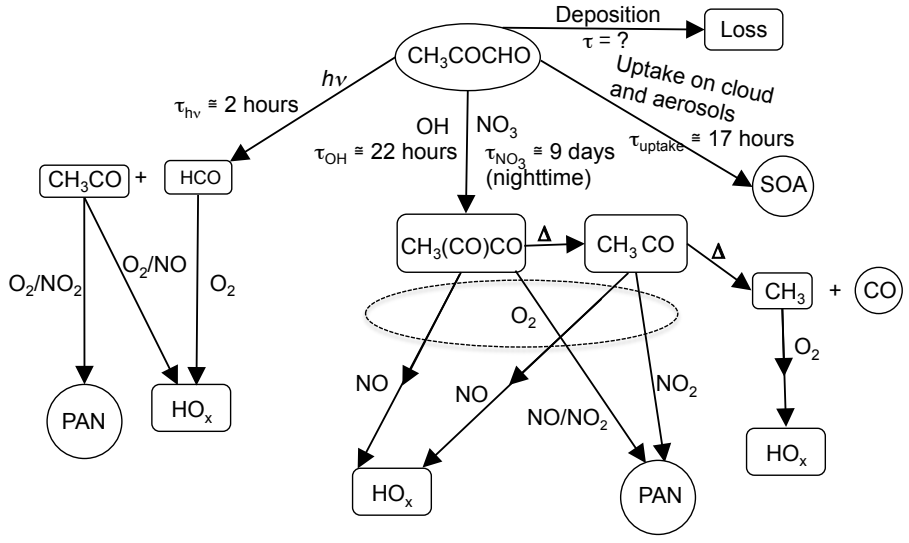


**Fig. 1.** Simplified atmospheric degradation scheme for methylglyoxal highlighting loss via UV photolysis, OH radical reaction, $NO_3$ radical reaction, and cloud and aerosol uptake. Approximate atmospheric lifetimes are included (see text for details).

et al., 2003; Ho et al., 2006; Liggio and McLaren, 2003; Moortgat et al., 2002).

The general atmospheric degradation scheme for methylglyoxal given in Fig. 1 shows that the competition between its reaction with the OH radical and its UV photolysis plays an important role in determining $HO_x$ production, which effects the oxidation capacity of the atmosphere, and the $CH_3C(O)OONO_2$ (PAN) yield, which impacts ozone production in remote locations (Atkinson et al., 2006; Baeza-Romero et al., 2007; Staffelbach et al., 1995). Reaction with the OH radical

$$\mathrm{OH}+\mathrm{CH_3COCHO} \rightarrow \mathrm{CH_3COCO}+\mathrm{H_2O} \quad -27\,\mathrm{kcal\,mol^{-1}} \quad \text{(R1a)}$$

$$\rightarrow \mathrm{CH_2COCHO}+\mathrm{H_2O} \quad -20\,\mathrm{kcal\,mol^{-1}} \quad \text{(R1b)}$$

leads to no net $HO_x$ radical production, while degradation via UV photolysis produces $HO_x$ (Atkinson et al., 2006)

$$\mathrm{CH_3COCHO}+h\nu \rightarrow \mathrm{CH_3CO}+\mathrm{HCO} \quad 387\,\mathrm{nm} \quad \text{(R2a)}$$

$$\rightarrow \mathrm{CH_4}+2\mathrm{CO} \quad \text{All} \quad \text{(R2b)}$$

$$\rightarrow \mathrm{CH_3CHO}+\mathrm{CO} \quad \text{All} \quad \text{(R2c)}$$

$$\rightarrow \mathrm{CH_3COCO}+\mathrm{H} \quad 380\,\mathrm{nm} \quad \text{(R2d)}$$

where the heats of reaction, $\Delta_r H^0$, and photolysis thresholds were calculated using available thermochemical parameters (Sander et al., 2006). $CH_3COCO$ radical formed in channels (R1a) and (R1d) spontaneously dissociates to $CH_3CO$ and CO in $<15$ µs (Green et al., 1990). $CH_3CO$ radical from channel 1a has sufficient energy to dissociate further to $CH_3$ and CO (Baeza-Romero et al., 2007). PAN, which enables the long-range transport of $NO_x$ ($NO_x$ = NO + $NO_2$) and ultimately ozone production in remote areas, is an end-product of both the OH reaction and UV photolysis mechanisms. It is important to quantify the degradation pathways to fully evaluate the impact of methylglyoxal on tropospheric chemistry.

Several studies of the rate coefficient for Reaction (R1), $k_1$, have been reported to date with room temperature values falling in the range $(7–16) \times 10^{-12}$ cm$^3$ molecule$^{-1}$ s$^{-1}$ (Baeza-Romero et al., 2007; Kleindienst et al., 1982; Plum et al., 1983; Tyndall et al., 1995). Rate coefficient data at atmospherically relevant temperatures, $\leq$298 K, is, however, more limited. In fact, only one study has reported rate coefficient data at temperatures below 260 K (Baeza-Romero et al., 2007). The current IUPAC kinetic data evaluation recommends $k_1(T) = 1.9 \times 10^{-12}$ exp$((575 \pm 300)/T)$ cm$^3$ molecule$^{-1}$ s$^{-1}$ for use in atmospheric models (Atkinson et al., 2006). The large uncertainty in the activation energy, *E/R*, is primarily due to a lack of experimental data for the temperature dependence of Reaction (R1). Additional measurements of $k_1(T)$, particularly at reduced temperatures, are therefore warranted and were addressed in the present study.

Nighttime atmospheric loss processes of methylglyoxal and glyoxal are also of interest for modeling tropospheric chemistry and possible SOA formation, but at present are not well characterized. The reaction of methylglyoxal and glyoxal with $NO_3$ and $O_3$ as well as their heterogeneous processing on atmospheric aerosol represent the most likely nighttime loss processes. Currently there are no experimental kinetic data available for the $NO_3$ radical reaction with glyoxal and methylglyoxal

$$NO_3 + (HCO)_2 \rightarrow \text{Products} \quad \text{(R3)}$$

$$NO_3 + CH_3COCHO \rightarrow \text{Products} \quad \text{(R4)}$$

At present, atmospheric chemistry models rely on estimated rate coefficient values for Reactions (R3) and (R4) (Myriokefalitakis et al., 2008). In the present study, rate coefficients for the reaction of the $NO_3$ radical with glyoxal and methylglyoxal are reported.

## 2 Experimental details

Rate coefficients for the gas-phase reaction of OH with $CH_3COCHO$ were measured as a function of temperature (211–373 K) and pressure (100–200 Torr in He and $N_2$) by producing OH via pulsed laser photolysis (PLP) and measuring its temporal profile using laser-induced fluorescence (LIF). Rate coefficients for the reactions of $NO_3$ with glyoxal ($k_3$) and methylglyoxal ($k_4$) were measured at 630 Torr and 296 K via a relative rate technique using Fourier transform infrared spectroscopy (FTIR) to monitor the extent of reaction. $k_3(T)$ was also measured at 296 and 353 K in a flow tube reactor at 3–6 Torr that was coupled to a chemical ionization mass spectrometer (FT-CIMS). The experimental apparatus and methods used have been described in detail elsewhere (Talukdar et al., 1995, 2003; Vaghjiani and Ravishankara, 1989; Zhu et al., 2008). Here, we only present the essentials needed to understand the present work.

### 2.1 OH reaction rate coefficients

Rate coefficients were measured under pseudo-first-order conditions in OH, $[OH] \ll [CH_3COCHO]$ using the PLP-LIF experimental apparatus. A schematic of the apparatus is provided in the Supplement. The key components of the apparatus were (1) a temperature controlled reactor where OH was produced by pulsed laser photolysis and its temporal profile measured by laser-induced fluorescence, (2) pulsed lasers used to generate and detect OH, (3) a gas handling manifold, and (4) UV and infrared absorption setups to determine the methylglyoxal concentration on-line using UV absorption at 184.9 nm and Fourier transform infrared (FTIR) spectroscopy.

OH radicals were produced by the 248 nm pulsed laser (KrF, excimer laser) photolysis of $H_2O_2$

$$H_2O_2 + h\nu \rightarrow 2OH \quad \text{(R5)}$$

for kinetic measurements at temperatures $\geq$255 K. For temperatures $<$255 K condensation of $H_2O_2$ interfered with the rate coefficient measurements. For kinetic experiments performed at temperatures between 211 and 373 K OH was produced in the 248 nm pulsed photolysis of *tert*-butyl hydroperoxide, $(CH_3)_3COOH$

$$(CH_3)_3COOH + h\nu \rightarrow \text{products} + OH \quad \text{(R6)}$$

Photolysis of $HNO_3$ at 248 nm was also used in limited cases. The initial OH radical concentration, $[OH]_0$, was estimated to be in the range of $(0.3–2.7) \times 10^{11}$ molecule cm$^{-3}$ based on the photolyte concentration, absorption cross section and quantum yield, and the photolysis laser fluence (Baasandorj et al., 2010; Sander et al., 2011; Taylor et al., 2008). The OH radical was detected by fluorescence following excitation in the $A^2\Sigma^+(v=1) \leftarrow X^2\Pi(v=0)$ transition at 282 nm using the frequency doubled output from a pulsed Nd:YAG pumped dye laser (Vaghjiani and Ravishankara, 1989).

The OH decay obeyed the integrated rate expression

$$\ln\left(\frac{[OH]_t}{[OH]_0}\right) = -(k_1[CH_3COCHO] + k_d)t = -k't \quad (1)$$

where $[OH]_t$ is the OH concentration at time $t$ and $k_d$ is the first-order rate coefficient for OH loss in the absence of $CH_3COCHO$, which is primarily due to reaction with the OH precursor and diffusion out of the detection volume. $k'$ was measured for a range of $[CH_3COCHO]$ at each temperature and pressure and $k_1(T)$ was determined from the slope of $k'$ versus $[CH_3COCHO]$. Typical values of $k_d$ were in the range 50–500 s$^{-1}$ where the actual value depended on the OH precursor used and its concentration. Values of $k_d$ measured in the absence of methylglyoxal were in excellent agreement with those obtained from the intercept of $k'$ versus $[CH_3COCHO]$.

Methylglyoxal was introduced into the PLP-LIF gas flow from dilute gas mixtures of methylglyoxal in He (0.5–2.0 %) that were prepared manometrically in darkened 12 l Pyrex bulbs at total pressures of $\sim$1000 Torr. The methylglyoxal concentration in the LIF reactor was determined using the measured gas flow rate in addition to on-line optical absorption measurements. The UV absorption of methylglyoxal was measured using an Hg Pen-Ray lamp light source, a 100 cm long (2.5 cm dia.) absorption cell, a 184.9 nm narrow band-pass filter, and a solar blind phototube detector. Infrared absorption spectra were recorded between 500 and 4000 cm$^{-1}$ at a spectral resolution of 1 cm$^{-1}$ using a Fourier transform spectrometer. A multi-pass absorption cell (485 cm optical path length, 550 cm$^3$ volume, and KBr windows) was used for all infrared measurements. UV absorption was measured before the LIF reactor, while infrared absorption spectra were measured either before or after the LIF reactor. The methylglyoxal concentration in the LIF reactor determined from the optical measurements was scaled for gas flow dilution and differences in temperature and pressure between the LIF reactor and the absorption cells. The methylglyoxal concentration was varied over the range (5–174) $\times 10^{13}$ molecule cm$^{-3}$ during the course of the kinetic measurements.

### 2.2 Absorption cross-section measurements

Infrared and UV (184.9 nm) absorption cross sections of $CH_3COCHO$ were determined as part of this work. Cross sections of $CH_3COCHO$ at 296 K were determined using Beer-Lambert law, $A = L\sigma$ [$CH_3COCHO$], from a linear least-squares analysis of the measured absorbance versus [$CH_3COCHO$]. The infrared (IR) and ultraviolet (UV) measurements were made simultaneously using a multi-pass cell (path length = 485 cm) for IR and 100 cm path length for UV. The cells were connected in series and the gas flow velocity was varied as part of the measurements. Cross sections were measured both under static fill and flowing conditions with the $CH_3COCHO$ concentration determined from absolute pressure measurements of manometrically prepared $CH_3COCHO$/He mixtures (0.5–2 %). At least 10 different $CH_3COCHO$ concentrations, varied over at least an order of magnitude, were used in the cross section determinations. No difference was observed at different flow velocities or the direction of the flow, which indicates no loss of methylglyoxal in the flow through the apparatus.

The absorption cross section of $CH_3COCHO$ at 184.9 nm was determined to be $(5.21 \pm 0.16) \times 10^{-18}$ cm$^2$ molecule$^{-1}$ where the error limit represents $2\sigma$ precision of the measurements.

The infrared absorption spectrum of methylglyoxal agrees with those reported in earlier studies and is given in the Supplement (Plum et al., 1983; Tuazon and Atkinson, 1989). The infrared cross sections determined using methylglyoxal samples obtained from different synthesis agreed to within 2 %. The integrated band intensities and the peak cross sections obtained in this work are given in Table 1. The methylglyoxal infrared cross sections obtained in this work are 8 to 15 % greater, depending on the spectral region, than those reported by Staffelbach et al. (1995). After our ACPD paper was published, an IR absorption study of several dicarbonyls was published (Profeta et al., 2011). The agreement in absolute intensities between their results and the present work is excellent (within 3 %).

### 2.3 $NO_3$ reaction rate coefficients

Two independent experimental techniques were used to determine $k_3$ and $k_4$ (a) an absolute method using a flow tube reactor coupled to a chemical ionization mass spectrometer (FT-CIMS) to measure $k_3$ at 296 and 353 K and (b) a relative rate technique using Fourier transform infrared spectroscopy (RR-FTIR) to measure $k_3$ and $k_4$ at 296 K.

#### 2.3.1 Flow tube – chemical ionization mass spectrometer (FT-CIMS) method

Details of the experimental apparatus is given in a previous publication from this laboratory (Talukdar et al., 2003). The temperature regulated halocarbon wax coated flow tube reactor was a 150 cm long Pyrex tube, 2.54 cm i.d., with a moveable injector. The outside of the moveable injector (120 cm long, 0.64 cm o.d.) was also coated with halocarbon wax. The reaction zone of the flow tube was ∼50 cm. The reaction time in the flow tube was between 16 and 85 ms; total gas flow rates of 10 to 25 STP cm$^3$ s$^{-1}$ at pressures between 2 and 6 Torr. A chromel-alumel thermocouple, inserted through the injector was used to measure the temperature of the gas in the reaction zone; the variation in the temperature along the reaction zone was ≤1 K.

Rate coefficients were measured under pseudo-first-order conditions in $NO_3$, [Glyoxal]/$[NO_3]_0 \sim 1000$, with $NO_3$ radicals produced by the thermal decomposition of $N_2O_5$ at 400 K (Rudich et al., 1996). $NO_3$ was introduced either through the moveable injector or through a side arm into the flow tube. Glyoxal was added to the flow tube opposite to the $NO_3$ addition point. The initial $NO_3$ radical concentration in the flow tube was in the range $(1–5) \times 10^{11}$ molecule cm$^{-3}$. With a signal-to-noise ratio of ∼1000 and a detection sensitivity of $\sim 2 \times 10^8$ molecule cm$^{-3}$ for one second integration, changes in [$NO_3$] of less than 1 % could be measured.

The effluent of the flow tube passed through a Pyrex valve into the ion flow tube, at ∼0.5 Torr, approximately 50 cm downstream of the ionization source. $N_2O_5$ and $NO_3$ were detected by a quadrupole mass spectrometer as $NO_3^-$ following their reaction with $I^-$ reagent ion.

The variation of $NO_3$ concentration with the relative injector position was used to derive the pseudo-first-order rate coefficient, $k'$, which was measured at various glyoxal concentrations to obtain $k_3$

$$k' = k_3[(CHO)_2] + k_w \quad (2)$$

where $k_w$ (typically in the range: ∼0.2–0.5 s$^{-1}$) represents the pseudo-first-order wall loss of $NO_3$. A linear least-squares fit of $k'$ vs. [glyoxal] yielded the second-order rate coefficient, $k_3$, which was determined at 296 and 353 K.

#### 2.3.2 Relative rate method (RR-FTIR)

A relative rate method was used to determine $k_3$ and $k_4$ using ethene ($CH_2 = CH_2$) and iso-butane ($(CH_3)_2CHCH_3$) as reference compounds. In this method, if the reactant of interest, $R$, and a reference compound (Ref) are removed solely by reaction with $NO_3$

$$NO_3 + R \rightarrow \text{products}, \; k_R \quad \text{(R7)}$$

$$NO_3 + \text{Ref} \rightarrow \text{products}, \; k_{\text{Ref}} \quad \text{(R8)}$$

the ratio of their reaction rate coefficients, $k_R/k_{\text{Ref}}$, is given by

$$\frac{k_R}{k_{\text{Ref}}} = \frac{\ln([R]_0/[R]_t)}{\ln([\text{Ref}]_0/[\text{Ref}]_t)} \quad (3)$$

where the subscripts 0 and $t$ refer to the initial reactant concentration and its concentration at time $t$. The slope of

**Table 1.** Infrared absorption band strengths and peak cross sections of methylglyoxal, $CH_3COCHO$, measured in this work at 296 K.

| | Staffelbach et al. (1995) | This work* |
|---|---|---|
| Integration range ($cm^{-1}$) | Band Strength ($10^{-18}$ $cm^2$ $molecule^{-1}$ $cm^{-1}$) | |
| 1296–1600 | – | $9.27 \pm 0.18$ |
| 1600–1880 | – | $30.1 \pm 0.40$ |
| 2780–2880 | – | $10.01 \pm 0.21$ |
| Peak Position ($cm^{-1}$) | Peak cross section ($10^{-19}$ $cm^2$ $molecule^{-1}$) | |
| 1374 | 1.46 | $1.66 \pm 0.04$ |
| 1737 | 6.65 | $7.23 \pm 0.13$ |
| 2835 | 2.75 | $3.22 \pm 0.06$ |

* The uncertainties are $2\sigma$ from the precision of the linear least-squares analysis of the integrated absorbance versus concentration.

$\ln([R]_0/[R]_t)$ vs. $\ln([\text{Ref}]_0/[\text{Ref}]_t)$ yields $k_R/k_{\text{Ref}}$ from which $k_R$ is determined provided $k_{\text{Ref}}$ is known.

Experiments were carried out in a 22 l Pyrex reactor under dark conditions at 296 K. Experiments were performed by first adding $N_2O_5$ to the reactor by flowing zero air over a solid $N_2O_5$ sample at 230 K. The reactant and reference compounds were then added to the reactor from dilute mixtures; 0.1 % ethene/$N_2$, 2–6 % glyoxal/He or 2 % methylglyoxal/He. Synthetic air was then added to bring the reactor total pressure to 630 Torr. The initial concentrations in the reactor were: $[N_2O_5] \sim 3.0 \times 10^{15}$ molecule $cm^{-3}$, and $[CH_2=CH_2]$, [glyoxal] or [methylglyoxal] of $\sim 1 \times 10^{15}$ molecule $cm^{-3}$.

$NO_3$ radicals were produced in situ by the thermal decomposition of $N_2O_5$

$$NO_3 + NO_2 + M \rightleftharpoons N_2O_5 + M \quad \text{(R9)}$$

where $k_{-9}$(296 K, 630 Torr) = 0.04 $s^{-1}$ and $K_{eq}$(296 K) = $2.9 \times 10^{-11}$ $cm^3$ $molecule^{-1}$ (Sander et al., 2011). The reaction was monitored by periodically transferring a portion of the reaction mixture from the reactor into the multi-pass absorption cell of the FTIR. An experiment typically lasted ~4 h with the contents of the reactor sampled every 30 min. In the data analysis the reactant and reference compound concentrations were corrected for the small change in reactor pressure, ~3 % at each stage of sampling.

### 2.4 Materials

He (UHP, 99.999 %), $N_2$ (UHP, >99.99 %), and $O_2$ (UHP, >99.99 %) were used as supplied. Concentrated $H_2O_2$ (>95 %) was prepared by bubbling $N_2$ for several days through a sample initially at 60 wt %. A small flow of bath gas was passed through the $H_2O_2$ bubbler, which was then diluted by the main bath gas flow before entering the reactor. The $H_2O_2$ reservoir was kept at 273 K during the kinetic measurements to avoid condensation of $H_2O_2$ in the reactor. A *tert*-butylhydroperoxide solution (70 % in water) was degassed and used without further purification. A small flow of $N_2$ or He bath gas was bubbled through the solution at 273 K to sweep *tert*-butylhydroperoxide into the main gas flow. $N_2O_5$ was synthesized by the reaction of ozone with $NO_2$ as described elsewhere (Papadimitriou et al., 2011; Rudich et al., 1996).

Methylglyoxal samples were prepared from commercial 40 % aqueous solutions. A 25 ml aliquot of the solution was transferred into a 500 ml round bottom flask partially filled with small pieces of glass tubes. The flask was kept in the dark and pumped on for 16–20 h to remove water. The remaining viscous liquid was then covered with ~6 g of $P_2O_5$ and heated to 323–333 K. A yellow oily liquid was collected in a trap at 195 K for ~5 min. The distillate was then pumped on for approximately one hour with the sample at dry ice temperature. The trap was then quickly warmed to ~283 K and the volatile impurities, such as formaldehyde, were pumped off and the sample re-cooled to dry ice temperature. This process was repeated three times. No FTIR detectable impurities were observed in the final sample. A formaldehyde impurity upper limit was estimated to be <1 %. Dilute mixtures of methylglyoxal in a He bath gas (0.5–2 %) were prepared in a darkened 12 l Pyrex bulb. The dilute gas mixture composition was tested periodically using FTIR and found to be stable for a period of several weeks. After ~3 weeks of storage weak unidentified infrared absorption peaks in the range 800–1000 $cm^{-1}$ were observed.

Glyoxal monomer was prepared from the solid trimeric-dihydrate using the methods described elsewhere (Volkamer et al., 2005; Feierabend et al., 2008). The vapor pressure of glyoxal and methylglyoxal were measured to be ~0.03 Torr (~$1.5 \times 10^{15}$ molecule $cm^{-3}$) and 0.016 Torr (~$8.0 \times 10^{14}$ molecule $cm^{-3}$), respectively, at 195 K.

Gas flow velocities through the reaction zone in the LIF reactor were in the range 6–15 cm $s^{-1}$, which ensured a fresh gas mixture for each photolysis laser pulse. Gas flows were measured using calibrated electronic mass flow meters. Pressures were measured using calibrated 10, 100, and 1000 Torr

**Table 2.** Summary of experimental conditions and measured rate coefficients for the OH + $CH_3COCHO$ (methylglyoxal) reaction, $k_1(T)$.

| $T$ (K) | Pressure (Torr) | Bath Gas | $O_2$ ($10^{16}$ molecule $cm^{-3}$) | Flow velocity (cm $s^{-1}$) | OH precursor[a] and concentrations ($10^{14}$ molecule $cm^{-3}$) | Photolysis laser fluence (mJ $cm^{-2}$ $pulse^{-1}$) | $[OH]_0$ ($10^{11}$ molecule $cm^{-3}$) | $[CH_3COCHO]$ ($10^{14}$ molecule $cm^{-3}$) | $k_1(T)$[b] ($10^{-11}$ $cm^3$ $molecule^{-1}$ $s^{-1}$) |
|---|---|---|---|---|---|---|---|---|---|
| 211 | 120 | $N_2$ | – | 6-12 | *tert*-BHP/1.3 | 8 | 0.3 | 2.7–14.0 | $2.77 \pm 0.14$ |
| 213 | 110 | $N_2$ | – | 11 | *tert*-BHP/1.4 | 11 | 0.4 | 0.6–6.4 | $2.55 \pm 0.08$ |
| 229 | 110 | $N_2$ | – | 7–11 | *tert*-BHP/1.9 | 8 | 0.4 | 1.0–6.6 | $2.25 \pm 0.04$ |
| 229 | 120 | $N_2$ | – | 11.9 | *tert*-BHP/1.7 | 7 | 0.3 | 1.0–6.4 | $2.26 \pm 0.04$ |
| 255 | 110 | $N_2$ | 0–6.4 | 7–15 | $H_2O_2$/0.5 | 7 | 0.8 | 1.3–9.2 | $1.84 \pm 0.02$ |
| 271 | 110 | $N_2$ | 0–5.3 | 11 | $H_2O_2$/1.4 | 7 | 2.0 | 1.0–7.6 | $1.53 \pm 0.02$ |
| 271 | 110 | $N_2$ | 0–5.2 | 7–14 | $HNO_3$/7.2 | 5 | 0.9 | 1.0–7.8 | $1.52 \pm 0.04$ |
| 271 | 112 | $N_2$ | – | 7–14 | *tert*-BHP/1.2 | 8.4 | 0.3 | 1–5.2 | $1.57 \pm 0.06$ |
| 295 | 108 | He | – | 9 | $H_2O_2$/0.5 | 4.5 | 0.44 | 0.5–3.0 | $1.29 \pm 0.06$ |
| 295 | 102 | He | – | 8 | $H_2O_2$/0.6 | 4.5 | 0.6 | 1.1–9.1 | $1.24 \pm 0.02$ |
| 295 | 210 | $N_2$ | 0-5.4 | 12 | $H_2O_2$/0.8 | 5–16 | 0.9–2.7 | 1.6–11.5 | $1.28 \pm 0.04$ |
| 295 | 220 | $N_2$ | 0–6.5 | 7 | $H_2O_2$/0.7 | 5.6 | 0.9 | 2.2–14.0 | $1.30 \pm 0.04$ |
| 315 | 195 | $N_2$ | 0–5.3 | 9 | $H_2O_2$/0.4 | 5.6 | 0.4 | 1.8–13.0 | $1.10 \pm 0.028$ |
| 333 | 193 | $N_2$ | 0–5.3 | 10.0 | *tert*-BHP/1.7 | 7.6 | 0.34 | 1.9–14.1 | $0.954 \pm 0.024$ |
| 352 | 210 | $N_2$ | 0–5.3 | 9.6 | *tert*-BHP/1.9 | 7.6 | 0.40 | 2.0–14.4 | $0.887 \pm 0.014$ |
| 355 | 216 | $N_2$ | 0–5.4 | 9.0 | $H_2O_2$/1.1 | 5.0 | 1.2 | 2.0–17.4 | $0.914 \pm 0.014$ |
| 373 | 212 | $N_2$ | 0–5.0 | 9.8 | *tert*-BHP/1.5 | 7.4 | 0.3 | 2.3–15.9 | $0.78 \pm 0.022$ |
| 373 | 210 | $N_2$ | 0–5.0 | 11.0 | $H_2O_2$/0.6 | 6.5 | 0.9 | 1.7–14.0 | $0.831 \pm 0.008$ |

[a] *tert*-BHP: tertiary butyl hydroperoxide, $(CH_3)_3COOH$.

[b] The quoted uncertainties are $2\sigma$ from the precision of linear least-squares data fits of pseudo-first order rate coefficients, $k'$, versus the concentration of methylglyoxal.

capacitance manometers. The photolysis and probe lasers were operated at 10 Hz.

## 3 Results and discussion

Rate coefficients for the OH reaction with methylglyoxal, $k_1(T)$, and the $NO_3$ reaction with glyoxal ($k_3$) and methylglyoxal ($k_4$) are presented separately below.

### 3.1 OH + $CH_3COCHO$

A summary of the experimental conditions used in our rate coefficient measurements and the obtained $k_1(T)$ values are given in Table 2. A potential complication in the rate coefficient measurement of Reaction (R1) arises due to the unavoidable formation of the $CH_3CO$ radical as a secondary reaction product. The $CH_3CO$ radical is known to react with $O_2$ to produce OH radicals as a reaction product (Baeza-Romero et al., 2007; Tyndall et al., 1995)

$$CH_3CO + O_2 + M \rightarrow OH + \text{Products} \quad \text{(R10a)}$$

$$\rightarrow CH_3C(O)O_2 + M \quad \text{(R10b)}$$

which could possibly influence the determination of $k_1(T)$ under certain conditions. In this work, rate coefficients were measured at pressures >100 Torr with He and $N_2$ bath gases, where the OH radical yield in Reaction (R10) is known to be small (Tyndall et al., 1995). The OH yield in Reaction (R10) in a $N_2$ bath gas is less than in He. The formation of OH was observed, as expected, in test experiments performed with and without $O_2$ added to the reaction mixture. OH radical temporal profiles measured at low pressure (20–50 Torr, He) were found to be non-exponential indicating regeneration of OH on the time scale of the measurement. The measured OH temporal profiles were exponential within the precision of the measurement when ~2 Torr of $O_2$ was added to the reaction mixture. The measured pseudo-first-order rate coefficient in the presence of $O_2$ was, however, ~13 % less at 50 Torr (He) than that obtained in the absence of added $O_2$. This is consistent with ~13 % OH generation via Reaction (R10) (Talukdar et al., 2006). We assume that the non-exponential behavior observed in the absence of added $O_2$ may in part be due to a small $O_2$ impurity in the system. At greater bath gas pressure, >100 Torr $N_2$, the OH temporal profiles were exponential, with and without added $O_2$, and yielded indistinguishable pseudo-first-order decay rate coefficients, within the precision of the measurement (~2 %). This was the case over the entire temperature range, 211–373 K, included in our study. The rate coefficients for Reaction (R1) reported in this work were measured at total pressures >100 Torr where OH regeneration was negligible.

Figure 2 shows representative OH temporal profiles measured at 295 K in 210 Torr $N_2$ and at 211 K in 120 Torr $N_2$ obtained while using 248 nm photolysis of $H_2O_2$ and *tert*-butyl hydroperoxide, respectively, as the OH radical source. The OH temporal profiles were measured with high precision over two order of magnitude decay in the OH signal in most cases.

Figure 3 summarizes the $k'$ data obtained for a range of experimental conditions at temperatures between 211 and 373 K. The pseudo-first-order rate coefficients obtained with both OH radical sources were observed to

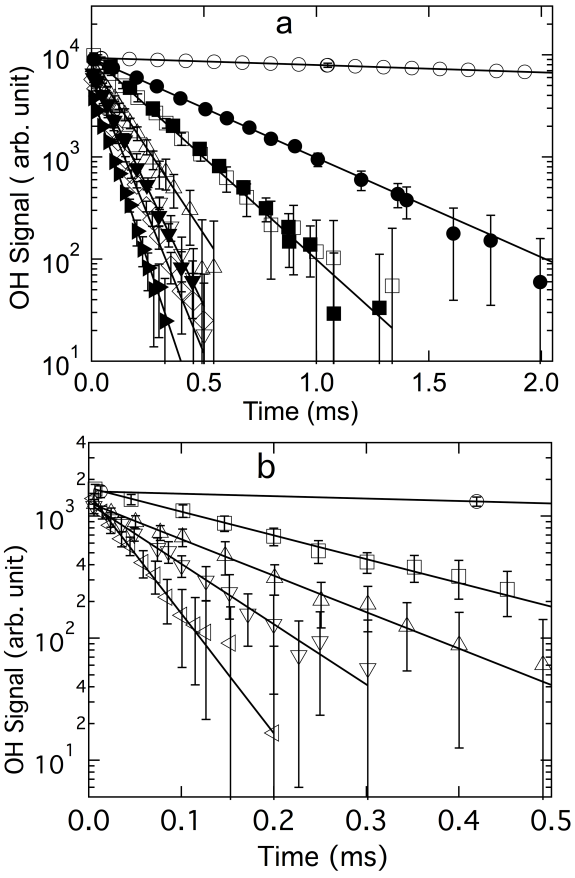


**Fig. 2.** Representative OH temporal profiles obtained at 295 K using $H_2O_2$ photolysis at 248 nm (upper panel) and at 211 K using tert-butyl hydroperoxide (lower panel) as the OH radical sources. [$CH_3COCHO$] ($10^{14}$ molecule $cm^{-3}$); open symbols: [$O_2$] = 0.0; filled symbols: [$O_2$] = $5.4 \times 10^{16}$ molecule $cm^{-3}$; upper panel: 0.0 (◯), 1.64 (●), 3.32 (■, □), 5.81 (△), 7.91 (▽, ▼), 9.25 (◊), 11.54 (►); lower panel: 0.0 (◯), 1.23 (□), 2.15 (△), 3.66 (▽), 7.78 (◃). Lines in **(a)** and **(b)** are fits of the data to Eq. (1). The OH profiles shown in the upper panel have been offset for clarity.

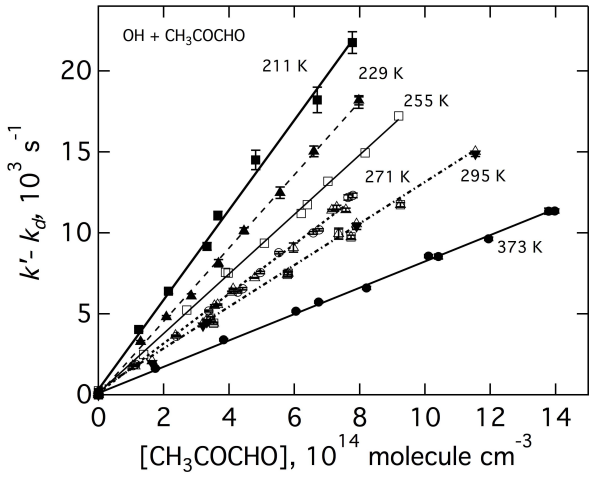


**Fig. 3.** Plots of $(k' - k_d')$ vs. [$CH_3COCHO$] where the data points were obtained using 248 nm photolysis of $H_2O_2$ for the OH radical source in the absence and presence of $O_2$. The error bars for individual $k' - k_d'$ values are $2\sigma$ precision obtained from fits as shown in Fig. 2. The lines are linear least-squares fits to all the data at each temperature.

be linearly dependent on [$CH_3COCHO$] at all temperatures. $k_1$ was obtained at each temperature by fitting all measured $(k' - k_d)$ values versus [$CH_3COCHO$] together using an un-weighted linear least-squares analysis. The room temperature rate coefficient obtained was $k_1(295\,K) = (1.29 \pm 0.05) \times 10^{-11}$ $cm^3$ molecule$^{-1}$ $s^{-1}$ where the quoted uncertainty is the $2\sigma$ (95 % confidence level) precision of the fit. The measured rate coefficients were independent of the bath gas (He or $N_2$) and total pressure, over the range 100–220 Torr. The measured rate coefficients were also independent of $[OH]_0$, varied by a factor of ∼7, concentrations of OH precursors by a factor of ∼2, and photolysis laser fluence by a factor of ∼3. The $k_1(T)$ values obtained at each temperature are given in Table 2 and plotted in Fig. 4. A weighted linear least-squares fit of $k_1(T)$ to the Arrhenius equation, $\ln(k_1(T)) = \ln(A) - E/(RT)$, yielded $k_1(T) = (1.74 \pm 0.09) \times 10^{-12}$ $\exp((590 \pm 12)/T)$ $cm^3$ molecule$^{-1}$ $s^{-1}$ where the quoted uncertainties are the $2\sigma$ precision of the fit and $\sigma_A = A\sigma_{\ln A}$.

### 3.1.1 Uncertainty evaluations

The absolute uncertainty in the measured rate coefficients originates from uncertainties in the measurement parameters, precision of the rate coefficient determinations, and potential systematic errors. Uncertainties arising from the pressure, temperature and flow rate measurements were small and contribute less than 2 % to the overall uncertainty in [$CH_3COCHO$]. The precision of the $k_1(T)$ measurements was very high with the error in the fits of the data to Eq. (1) being <5 % at 95 % confidence level.

A potential source of systematic error in our experiments involves the determination of the $CH_3COCHO$ concentration in the reactor. The uncertainty in the infrared and the UV absorption cross sections of methylglyoxal determined in this work was estimated to be ∼5 % at the 95 % confidence level. We estimate the uncertainty of [$CH_3COCHO$] in the reactor to be 8 %. The $CH_3COCHO$ concentration determined using FTIR before and after the reactor were in excellent agreement, <2 %, at all temperatures. This indicates that there was no measurable loss of methylglyoxal in the reactor due to decomposition at high temperature or condensation at low temperature. The measured first-order rate coefficients, $k'$, showed a linear dependence on [$CH_3COCHO$], even at the lowest temperature in our experiments (see Fig. 3). This observation confirmed that dimerization of methylglyoxal,

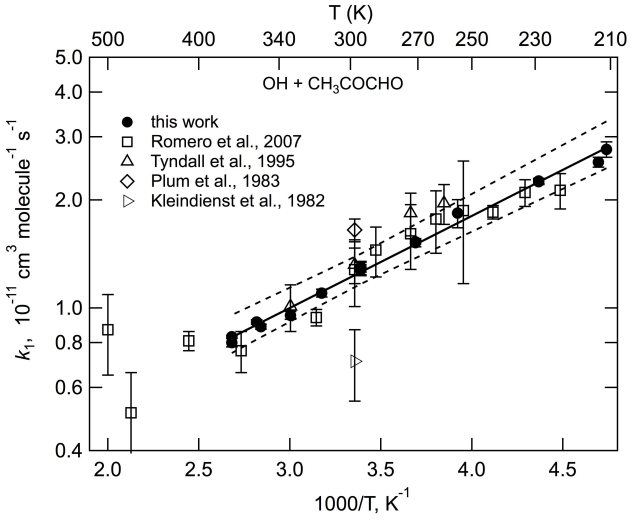


**Fig. 4.** Arrhenius plot for $k_1(T)$ (●) from this work. The solid line is linear least-squares fit that yields $k_1(T) = (1.74 \pm 0.20) \times 10^{-12}$ $\exp[(590 \pm 40)/T]$ cm$^3$ molecule$^{-1}$ s$^{-1}$. The error bars for the data are precision and systematic at the 95 % levels. Results obtained in previous experimental studies are included for comparison (see legend). The dashed lines represent the estimated $2\sigma$ error range in $k_1(T)$ calculated using the NASA/JPL (Sander et al., 2011) evaluation expression for errors $f(T) = f(298\,\mathrm{K})\exp\left|g(\frac{1}{T} - \frac{1}{298})\right|$ with $f(298\,\mathrm{K}) = 1.10$ and $g = 40$.

if any, which would most likely appear as a non-linear behavior of $k'$ vs. [$CH_3COCHO$], did not influence the kinetic measurement.

The presence of reactive impurities in the methylglyoxal sample could also influence the determination of $k_1$. The most likely impurities generated during the synthesis of methylglyoxal were CO ($\sim 2 \times 10^{-13}$ cm$^3$ molecule$^{-1}$ s$^{-1}$ at 298 K and 200 Torr $N_2$) and formaldehyde, $H_2CO$ ($9 \times 10^{-12}$ cm$^3$ molecule$^{-1}$ s$^{-1}$) where their OH reaction rate coefficients are given in parenthesis. CO, $H_2CO$, and other unidentified volatile impurities were removed from the sample by pumping on the methylglyoxal sample until their levels were below the FTIR detectable limit, as discussed earlier. At these levels CO and $H_2CO$ would not contribute significantly to the measured loss of OH at the temperatures included in this work. There was no significant loss of methylglyoxal in the prepared mixtures over a period of 3 weeks. In addition, the rate coefficients obtained with the older mixtures were identical, within the uncertainty of the measurements, to the values obtained with freshly prepared samples.

The absolute uncertainty in $k_1$ is estimated to be 10 % at the 95 % confidence level. Including the systematic error in the rate coefficient values yields $k_1(298\,\mathrm{K}) = (1.26 \pm 0.13) \times 10^{-11}$ cm$^3$ molecule$^{-1}$ s$^{-1}$ and $k_1(T) = (1.74 \pm 0.20) \times 10^{-12}$ $\exp((590 \pm 40)/T)$ cm$^3$ molecule$^{-1}$ s$^{-1}$.

### 3.1.2 Comparison with previous studies

A summary of previous Reaction (R1) rate coefficient results along with the parameters determined in this work is given in Table 3. The rate coefficient data from the previous studies, which extend over the temperature range 223–500 K, are included in Fig. 4 for comparison with the present work. The $k_1(298\,\mathrm{K})$ values reported by Baezo-Romero et al. (2007) and Tyndall et al. (1995) are in good agreement with our results, while Plum et al. (1983) report a value that is ∼30 % greater. The rate coefficient measured by Kleindienst et al. (1982) at 297 K is roughly a factor of 2 less than that reported here. The presence of significant levels of low reactivity impurities in their samples could have lead to lower measured rate coefficients. However, in the absence of a sample analysis, it is not clear why their $k_1$ value is significantly lower than obtained in the present work.

Baeza-Romero et al. (2007) and Tyndall et al. (1995) have reported on the temperature dependence of Reaction (R1). The data of Baeza-Romero et al. are in reasonable agreement with the present work, in the overlapping temperature range, but show more scatter. Their data for temperatures >366 K deviate greatly from their rest of the data, see Fig. 4. The larger scatter may in part be the result of the method used to extract values of $k_1$ from bi-exponential fits of their measured non-exponential OH temporal profiles. Bi-exponential fitting of simulated OH temporal profiles, under their conditions, confirmed that a larger uncertainty in the returned values of $k_1$ should be expected. On the other hand, the Arrhenius parameters reported by Baeza-Romero et al. agree very well with those derived from our data (Table 3).

The rate coefficient values reported by Tyndall et al. (1995) below 298 K are systematically greater than obtained in this work, leading to a substantially larger negative value of *E/R*. Tyndall et al. reported observing reversible sticking of methylglyoxal on the walls of their flow tube at temperatures <298 K, although it is not clear if this would account for the difference in the rate coefficients at low temperatures. Tyndall et al. (1995) reported a value of $k_1(298\,\mathrm{K})$ at low pressure (2–3 Torr) that agrees well with the present work and the Baeza-Romero et al. (2007) value. The agreement in $k_1(298\,\mathrm{K})$ over a broad range of pressure, 2–200 Torr, implies that there is no pressure dependence of Reaction (R1) under relevant atmospheric conditions.

Galano et al. (2004) calculated $k_1(T)$ using quantum chemistry and canonical variational transition state theory including small curvature tunneling and their values are included in Table 3 for comparison with the experimental results. The theoretically calculated value for $k_1(298\,\mathrm{K})$, $1.35 \times 10^{-11}$ cm$^3$ molecule$^{-1}$ s$^{-1}$, is in excellent agreement with that determined in this work and reported by Tyndall et al. (1995) and Baeza-Romero et al. (2007) (Table 2 and Fig. 4). However, the theoretically calculated temperature dependence, $E/R = -(1060 \pm 8)$, is much greater than that

**Table 3.** Summary of rate coefficient data, $k_1(T)$, for the reaction OH + $CH_3COCHO \rightarrow$ products.

| Reference | Rate Coefficient method[a] | OH radical source | [$CH_3COCHO$] method [a] | $T$ (K) | $P$ (Torr) | $k_1$(298 K) ($10^{-11}$ cm$^3$ molecule$^{-1}$ s$^{-1}$) | $A$ ($10^{-12}$ cm$^3$ molecule$^{-1}$ s$^{-1}$) | $E/R$ (K) |
|---|---|---|---|---|---|---|---|---|
| This work | PLP-LIF | $H_2O_2$ /248 nm<br>$HNO_3$/248 nm<br>$(CH_3)_3COOH$/248 nm | FTIR<br>Gas Flow<br>UV (184.9 nm) | 211–373 | 100–200 (He, $N_2$) | $1.26 \pm 0.13$ | $1.74 \pm 0.20$ | $-(590 \pm 40)$ |
| IUPAC (2006) | Evaluation | – | – | 220–410 | – | $1.3 \pm 0.20$ | 1.9 | $-(575 \pm 300)$ |
| Baeza-Romero et al. (2007) | PLP-LIF | $(CH_3)_3COOH$/248 nm | Gas Flow | 223–500 | 25–300 (He) | $1.28 \pm 0.27$ | $1.83 \pm 0.48$ | $-(560 \pm 70)$ |
| Tyndall et al. (1995) | DF-LIF | F + $H_2O$<br>H + $NO_2$ | Gas Flow<br>UV (220–340 nm) | 260–333 | 2–3 (He) | $1.32 \pm 0.30$ | $0.84 \pm 0.12$ | $-(830 \pm 50)$ |
| Plum et al. (1983) | RR-GC[b] | $CH_3ONO$/Air/NO (>290 nm) | DOAS | 296 | 760 (Air) | $1.65 \pm 0.12$ | – | – |
| Kleindienst et al. (1982) | FP-RF | $H_2O$ (>115 nm) | Gas Flow | 297 | 50–200 (Ar) | $0.71 \pm 0.16$ | – | – |
| Galano et al. (2004) | CVT/SCT Calculation | – | – | 200–500 | – | 1.35 | $0.393 \pm 0.011$ | $-(1060 \pm 8)$ |

[a] Method: PLP ≡ pulsed laser photolysis; LIF ≡ laser induced fluorescence; DF ≡ discharge flow; RF ≡ resonance fluorescence; FP ≡ flash photolysis; RR ≡ relative rate; FTIR ≡ Fourier transform infrared spectroscopy; GC ≡ gas chromatography; DOAS: differential optical absorption spectroscopy using a multi-pass White cell; CVT/SCT ≡ canonical variational theory (CVT) with small-curvature tunneling (SCT) corrections.

[b] cyclohexane reference with $k$(OH + cyclohexane) = $7.21 \times 10^{-12}$ cm$^3$ molecule$^{-1}$ s$^{-1}$.

reported in our study and by Baeza-Romero et al. (2007), but is somewhat closer to that reported by Tyndall et al. (1995).

Combining all the previous temperature dependent data in the overlapping temperature range with ours (211–373 K) except the data of Tyndall et al. (1995) at temperatures <298 K, we obtain, by weighted fit, the Arrhenius expression $k_1(T) = (1.82 \pm 0.33) \times 10^{-12}$ exp$[(577 \pm 50)/T]$ cm$^3$ molecule$^{-1}$ s$^{-1}$ The errors are at the 95 % confidence interval. Figure 4 includes the estimated error range in $k_1(T)$ calculated with the expression used in the NASA/JPL evaluation (Sander et al., 2011), $f(T) = f(298\,\mathrm{K})\exp\left|g(\frac{1}{T} - \frac{1}{298})\right|$, where $f(298\,\mathrm{K})$ is the uncertainty in the rate coefficient at 298 K, and $g$ is an additional uncertainty term to account for increased uncertainty at temperatures other than 298 K. We recommend $2\sigma$ values of $f(298\,\mathrm{K}) = 1.10$ and $g = 40$.

All available studies of Reaction (R1) report negative temperature dependence for $k_1$. The temperature dependence is slightly larger than reported for the reaction of OH with aliphatic aldehydes, e.g. $E/R = -330$ K for the OH + $CH_3CHO$ reaction at temperatures <300 K. Unlike glyoxal, which exhibits a weak non-Arrhenius behavior (Feierabend et al., 2008), Reaction (R1) follows an Arrhenius behavior, within the precision of the measurements, over the temperature range 211–373 K. The negative temperature dependence is consistent with Reaction (R1) proceeding via a hydrogen-bonded pre-reactive complex (Smith and Ravishankara, 2002). Theoretical calculations (Galano et al., 2004) found a reaction mechanism involving the formation of six- and seven-membered hydrogen-bonded adducts, [$CH_3COCHO\ldots OH$]*, as reaction intermediates in the H atom abstraction from the –CHO and –$CH_3$ groups, respectively. Galano et al. (2004) calculated the stabilization energies of the adducts for H abstraction from the –CHO and –$CH_3$ groups to be −3.28 and −2.82 kcal mol$^{-1}$, respectively. Although the stabilization energies of the adducts are very close, the calculated overall activation energy for aldehydic H-atom abstraction is negative (−2.39 kcal mol$^{-1}$), while that for H-atom abstraction from –$CH_3$ group is substantially positive (3.65 kcal mol$^{-1}$), leading to the former being the most probable pathway for reaction (Galano et al., 2004). The fraction of H atom abstraction from –$CH_3$ group could contribute at most ∼1 % of $k_1$ based on a comparison of the rate coefficients for the OH + $CH_3COCH_3$ (acetone) reaction, $k$(298 K) = $1.8 \times 10^{-13}$ cm$^3$ molecule$^{-1}$ s$^{-1}$, to that of the OH + $CH_3CHO$ reaction, $k$(298 K) = $1.5 \times 10^{-11}$ cm$^3$ molecule$^{-1}$ s$^{-1}$. In summary, experimental and theoretical results point to the formation of a pre-reactive complex and the abstraction of aldehydic H atom in Reaction (R1) leading to the observed negative activation energy.

### 3.2 $NO_3$ rate coefficients

#### 3.2.1 $NO_3$ + glyoxal

Figure 5 shows the measured values of $k'$ as a function of [glyoxal] obtained at 296 and 353 K using the absolute flow tube kinetic method. The measured pseudo-first-order rate coefficients, $k'$, are small, i.e. the rate coefficients for this reaction are small. The wall loss of $NO_3$ was 0.2–0.5 s$^{-1}$. The $k_3$ values obtained are $k_3$(296 K) = $(4.2 \pm 0.8) \times 10^{-16}$ and $k_3$(353 K) = $(7.9 \pm 3.6) \times 10^{-16}$ cm$^3$ molecule$^{-1}$ s$^{-1}$, which show an increase in reactivity with increasing temperature

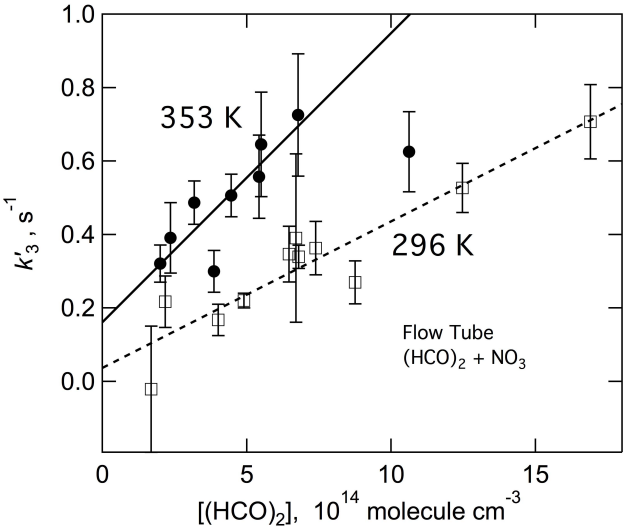


**Fig. 5.** Pseudo-first-order rate coefficients for the reaction of $NO_3$ + $(HCO)_2$ (glyoxal) obtained at 296 and 353 K using a fast flow-reactor with chemical ionization mass spectrometer (CIMS) detection of $NO_3$.

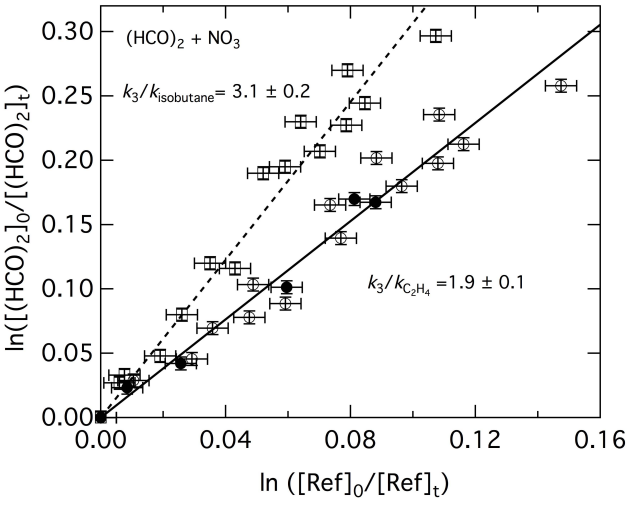


**Fig. 6.** Relative rate data for the $NO_3$ + $(HCO)_2$ (glyoxal) reaction at 296 K and 650 Torr (Syn. Air) with $C_2H_4$ and iso-butane as the reference compounds. The solid symbols represents the data obtained in the presence of $1.7 \times 10^{16}$ molecules $cm^{-3}$ of $CF_3CF=CHF$. The lines are linear least-squares fits of the data to Eq. (3), where the uncertainty is $2\sigma$ of the fit precision.

that is consistent with an abstraction reaction mechanism. However, due to the large uncertainty in $k_3$(353 K), the temperature dependence of $k_3(T)$ is not well established and it is not advisable to calculate the activation energy from these data points.

Figure 6 shows the results from the relative rate data for Reaction (R3) with $CH_2=CH_2$ as the reference compound. The rate coefficient ratio, $k_3/k_{Ref}$, obtained from a linear least-squares fit of the data to Eq. (3) is $1.9 \pm 0.2$, which yields $k_3$(296 K) = $(4.0 \pm 1.0) \times 10^{-16}$ $cm^3$ $molecule^{-1}$ $s^{-1}$. The possible formation of $HO_2$ radicals in the presence of $NO_3$ would lead to the formation of OH radicals, so experiments were also performed with an OH radical scavenger added to the reaction mixture. $CF_3CF$=CHF, $1.7 \times 10^{16}$ molecules $cm^{-3}$, was used as the OH scavenger due to its slow reaction with $NO_3$

$OH + CF_3CF=CHF \rightarrow$ Products $k(298\,K) = 1.3 \times 10^{-12}$ $cm^3$ $molecule^{-1}$ $s^{-1}$ (Papadimitriou et al., 2008) (R11)

$NO_3 + CF_3CF=CHF \rightarrow$ Products $k(295\,K) = 4.2 \times 10^{-18}$ $cm^3$ $molecule^{-1}$ $s^{-1}$ (Papadimitriou et al., 2011) (R12)

The measured $k_3$ was identical to that obtained in the absence of $CF_3CF$=CHF, which indicates that secondary OH radical chemistry did not influence the determination of $k_3$.

Experiments were performed using *iso*-butane as the reference compound to evaluate the possible interference of $NO_2$ and $N_2O_5$ reaction with ethene, $CH_2=CH_2$, as reference compound. $NO_2$ is known to react slowly with conjugated dialkenes (Barnes et al., 1990), while it is possible that $N_2O_5$ may react with alkenes. Therefore, $k_3$ was measured relative to iso-butane, a saturated hydrocarbon that is not likely to react with $N_2O_5$ or $NO_2$. The ratio of $k_3/k_{iso-butane}$ was determined to be $3.0 \pm 0.2$, which yields $k_3$ = $(3.3 \pm 0.85) \times 10^{-16}$ $cm^3$ $molecule^{-1}$ $s^{-1}$, which agrees, within the measurement uncertainty, with $k_3$ obtained using $C_2H_4$ as the reference. The apparatus and methods were also tested by measuring the rate coefficient ratios for the reaction of $NO_3$ with $CH_2=CH_2$ and iso-butane. The measured rate coefficient ratio for the reactions of $CH_2=CH_2$ and *iso*-butane with $NO_3$ was $1.53 \pm 0.38$. The measured ratio is lower than the recommended literature rate coefficient ratio of $1.91 \pm 0.50$, but falls within the current estimated uncertainties for these relatively slow reactions (Atkinson et al., 2006; Barnes et al., 1990; Canosa-Mas et al., 1988). Thus, it appears that there was no significant interference from the reactions of $NO_2$ or $N_2O_5$ in our experiments.

### 3.2.2 $NO_3$ + methylglyoxal

$k_4$ was measured using the relative rate technique with $CH_2=CH_2$ as the reference compound. Two sets of experiments were performed, using different methylglyoxal samples, with $CF_3CF=CHF$, $1.7 \times 10^{16}$ molecule $cm^{-3}$, added as an OH radical scavenger. The experimental results are shown in Fig. 7. The rate coefficient ratios, $k_4/k_{Ref}$, were determined from a linear least-squares fit of the data to Eq. (3) to be $2.9 \pm 0.5$ and $1.9 \pm 0.20$, where the quoted error limits are $2\sigma$ from the precision of the fit. Taking an average rate coefficient ratio of $2.4 \pm 1.0$ yields $k_4$(295 K) = $(5.1 \pm 2.1) \times 10^{-16}$ $cm^3$ $molecule^{-1}$ $s^{-1}$. The agreement

between the two experiments is rather poor when compared with the results obtained in the glyoxal + $NO_3$ reaction study given above. There is no explanation for the less reproducible results in the methylglyoxal experiments. The total reactant and reference compound losses (10–40 %) were relatively small over long time duration (4 h), which led to greater uncertainty in the measured rate coefficients.

### 3.2.3 Comparison of $NO_3$ rate coefficients

Rate coefficients for the reaction of $NO_3$ with glyoxal and methylglyoxal have not been reported previously. So here, we compare the present results with rate coefficients reported for aldehydes and ketones. The measured values of $k_3$ and $k_4$ from this work along with the rate coefficients for the acetaldehyde ($CH_3CHO$), formaldehyde (HCHO), and acetone reactions are listed in Table 4.

$k_3$ and $k_4$ are slow and similar in magnitude, $k_3$ is ∼20 % less than $k_4$. That is, although, glyoxal has two identical –C(O)H groups, its reactivity is actually slightly less than that of methylglyoxal. The reactivity could be attributed to the mutual deactivation of the aldehydic H atom reactivity by the adjacent electron withdrawing –C=O groups in glyoxal. The presence of the $–CH_3$ group in methylglyoxal may offset the electron withdrawing of the $\alpha$-carbonyl group thereby making the aldehydic H atom in methylglyoxal more reactive. This could, in part, account for the similar reactivity observed for glyoxal and methylglyoxal.

$k_3$ and $k_4$ are a factor of 5–7 less than the $NO_3$ + acetaldehyde reaction rate coefficient and, therefore, does not follow the same trend as in the OH radical reactivity. The room temperature OH rate coefficients of glyoxal and methylglyoxal are ∼40 % and ∼13 % less than that of acetaldehyde, which is $1.5 \times 10^{-11}$ cm$^3$ molecule$^{-1}$ s$^{-1}$ at 298 K. However, OH reaction rate coefficient of glyoxal compares well with that for formaldehyde (HCHO) and so does their $NO_3$ rate coefficients at room temperature. Based on the C-H bond energies for the –C(O)H group alone, the rate coefficients for the reaction of $NO_3$ radical with glyoxal and methylglyoxal would be greater than in acetaldehyde reaction. The estimated C-H bond energies of the –C(O)H group in glyoxal, methylglyoxal, formaldehyde, and acetaldehyde are 84.8 (Feierabend et al., 2009), 74, 88.6 and 89.4 kcal mol$^{-1}$, respectively (Sander et al., 2011; Galano et al., 2004). The measured rate coefficients do not seem to correlate with the bond energies, which is the most likely site for H atom abstraction because the C-H bond energy in the $–CH_3$ group (95.9 kcal mol$^{-1}$) is much greater and the barrier for H-abstraction from the $–CH_3$ group is higher, ∼7 kcal mol$^{-1}$ compared to ∼3 kcal mol$^{-1}$ from the –C(O)H group (D'Anna et al., 2003). For acetone, abstraction of H from the $CH_3$ group (–C-H bond energy = $96.4 \pm 1.0$ kcal mol$^{-1}$) (Espinosa-Garcia et al., 2003) is the only reaction pathway and is much slower than that from an aldehyde group –C(O)H group. Based on the thermochemical data, the major pathway in the reaction of $NO_3$ with methylglyoxal and acetaldehyde is expected to be abstraction of H from aldehydic group rather than from the $–CH_3$ group. Another factor that can influence the trend in the reactivity is the steric effect due to the much larger size of $NO_3$ radical compared to that of OH and could alter the reactivity trend. At present, it is not clear why $k_3$ and $k_4$ are substantially less than the $NO_3$ + acetaldehyde rate coefficient. High-level quantum chemistry calculations may shed some light on the reactivity trend of $NO_3$ radical with dicarbonyls and other aldehydes.

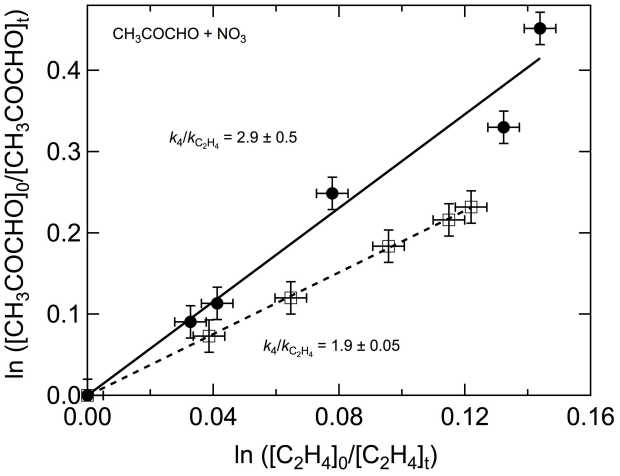


**Fig. 7.** Loss of methylglyoxal versus the reference compound, $C_2H_4$, in relative rate study for the $NO_3$ reaction at 296 K in 650 Torr of dry air.

## 4 Atmospheric implications

The primary atmospheric loss processes of methylglyoxal include reaction with the OH radical, UV/vis photolysis, and uptake on clouds and aerosols as outlined in Fig. 1. The reaction with Cl atoms is expected to be a minor loss process. Dry deposition losses are not well defined and often ignored. Recently, Karl et al. (2010) estimated, based on their laboratory and field measurements, and transport modeling, that the dry deposition of glyoxal and methylglyoxal can increase by ∼100 % and ∼20 % respectively compared to the previous estimates (Goldstein and Galbally, 2007; Hallquist et al., 2009; Zhang et al., 2002), which were used by Fu et al. (2008). In addition, ground-level measurements of oxygenated VOCs, particularly at night under high relative humidity scenarios, could be significantly impacted because of dry deposition. Dry and wet deposition, and the uptake on clouds and aerosols would be a function of location and likely to be significant nighttime loss processes. Fu et al. (2008) calculated the lifetime for methylglyoxal due to uptake on cloud and aerosol to be ∼17 h using the uptake coefficient for methylglyoxal on sulfuric acid solutions (50–85

**Table 4.** Comparison of $NO_3$ reaction rate coefficients for glyoxal and methylglyoxal measured in this work with those for other carbonyl compounds.

| Molecule | | $k$ ($10^{-16}$ cm$^3$ molecule$^{-1}$ s$^{-1}$) | Temperature (K) | Experimental method[a] | Reference |
|---|---|---|---|---|---|
| Glyoxal | $(HCO)_2$ | $4.2 \pm 0.8$ | 296 | FT-CIMS | This work |
| | | $4.0 \pm 1.0$[b] | 296 | RR | This work |
| | | $7.9 \pm 3.6$ | 353 | FT-CIMS | This work |
| Methylglyoxal | $CH_3COCHO$ | $5.1 \pm 2.1$[b] | 296 | RR | This work |
| Formaldehyde | HCHO | $5.5 \pm 0.9$ | | IUPAC Evaluation | Atkinson et al. (2006) |
| Acetaldehyde | $CH_3CHO$ | $27.4 \pm 0.7$[c] | 264-374 | FT-LIF | Dlugokencky and Howard (1989) |
| Acetone | $CH_3COCH_3$ | $0.09 \pm 0.03$ | 298 | SF-A | Boyd et al. (1991) |

[a] FT-CIMS: flow tube – chemical ionization mass spectrometry; RR: relative rate study; FT-LIF: flow tube – laser induced fluorescence detection of $NO_3$; SF-A: stopped flow coupled with $NO_3$ absorption measurement using a multi-pass cell.

[b] Relative to ethene.

[c] Fast flow laser induced fluorescence technique, $k(T) = (1.44 \pm 0.18) \times 10^{-12} \exp[-1860 \pm 300)/T]$ cm$^3$ molecule$^{-1}$ s$^{-1}$.

weight percent, $T$: 250–298 K) of $2.3 \times 10^{-3}$ reported by Zhao et al. (2006). On the other hand, Kroll et al. (2005) did not observe any net growth of ammonium sulfate aerosols in the presence of methylglyoxal at ∼50 % relative humidity. This is contrary to growth of particles in the presence of other dicarbonyls (Jang et al., 2003, 2005; Jang and Kamens, 2001). The large discrepancy could be due to the low RH (50–55 %) used in Kroll et al. study leading to low uptake. Fu et al. (2008) also calculated the global lifetime due to UV/vis photolysis and OH reaction to be 2.2 and 20 h, respectively. They also report a negligible effect of the $NO_3$ reaction on the atmospheric loss of methylglyoxal, even though a greater value of $k_3$ than measured in the present work was used in their analysis (Fu et al., 2008; Myriokefalitakis et al., 2008). Using the rate coefficient data from this work we estimate the lifetime with respect to $NO_3$ radical reactive loss would be ∼9 days, assuming ∼100 ppt $NO_3$. The $NO_3$ reaction, therefore, represents only a minor atmospheric loss process for methylglyoxal. Including dry deposition would decrease the lifetime of both dicarbonyls. However, their atmospheric loss would still be dominated by UV photolysis, OH reaction and uptake on clouds and aerosols.

The $CH_3COCO$ radical, which is formed in channel 1a with a ∼99 % yield (see the comparison section on OH reaction), decomposes promptly to $CH_3CO$ and CO under atmospheric conditions in <15 µs (Green et al., 1990). $CH_3CO$ radical has sufficient energy and as much as 40 % may dissociate further to $CH_3$ and CO even under atmospheric condition, thereby potentially reducing the effective yield of $CH_3CO$ (Baeza-Romero et al., 2007). $CH_3CO$ reacts with $O_2$ to form the peroxyacetyl (PA) radical, $CH_3C(O)O_2$, which in turn reacts with $NO_2$ to produce peroxyacetyl nitrate (PAN), $CH_3C(O)O_2NO_2$. The NO reaction with PA radical produces the $CH_3C(O)O$ radical and eventually $HO_x$. The atmospheric lifetime of PAN is predominantly controlled by its temperature dependent thermal decomposition and therefore highly altitude dependent. At altitudes >7 km PAN lifetimes can exceed several months. Thus, methylglyoxal, which has a short lifetime, leads to the formation of PAN, which is potentially much longer lived and can be transported longer distances and, therefore, impact atmospheric chemistry in remote locations. The loss of methylglyoxal due to the OH reaction leads to a null $HO_x$ production cycle if the products of the reaction do not leave the region. The OH reaction with methylglyoxal and the subsequent formation of PAN lead to the local loss of OH and $NO_2$ radicals. The transport of PAN to remote areas represents a $HO_x$ and $NO_2$ source. Thus, the OH reaction with methylglyoxal acts as local radical sink and remote source of $HO_x$. The PAN yield from the degradation mechanism of methylglyoxal will depend on the overall yield of $CH_3CO$ radical, the rate coefficients of the PA radical with NO and $NO_2$, which are $2.0 \times 10^{-11}$ cm$^3$ molecule$^{-1}$ s$^{-1}$ and $1.2 \times 10^{-11}$ cm$^3$ molecule$^{-1}$ s$^{-1}$ respectively, at 298 K and atmospheric pressure, and the $NO_2$/NO ratio (Atkinson et al., 2006). Plum et al. (1983) has qualitatively observed the formation of PAN following the irradiation of a mixture of methylglyoxal-$NO_x$-air using a solar simulator, but quantitative yields are currently not available. A direct measurement of molecular yields in the degradation of methylglyoxal under atmospheric conditions is needed.

UV/vis photolysis of methylglyoxal leads to a net production of $HO_x$ because $HO_x$ is not consumed in the initial methylglyoxal destruction step. PAN is also formed following photolysis of methylglyoxal via the same mechanism described above. The $NO_3$ reaction contributes negligibly (<1 %) to the loss of methylglyoxal, but would be a nighttime source of PAN. Uptake of methylglyoxal in clouds and aerosol would lead to the removal of reactive hydrocarbons from the atmosphere and reduce the oxidative capacity of the atmosphere and short-circuit PAN production. The heterogeneous loss of methylglyoxal would also have an impact on secondary aerosol formation.

The global lifetime of glyoxal due to loss via UV/visible photolysis, OH reaction, and uptake on cloud and aerosol are reported to be 4.9, 20, and 20 h, respectively (Chen et al., 2000; Fu et al., 2008; Staffelbach et al., 1995). An atmospheric modeling study, based on an estimated rate coefficient for the $NO_3$ + glyoxal reaction greater than obtained in this work, showed this loss process to be negligible (Fu et al., 2008). On the basis of the rate coefficient measured in this work the estimated glyoxal lifetime due to $NO_3$ reaction is ∼12 days for an $NO_3$ abundance of 100 pptv. The $NO_3$ reaction would contribute <1 % to the total loss of glyoxal.

**Supplementary material related to this article is available online at: http://www.atmos-chem-phys.net/11/10837/2011/acp-11-10837-2011-supplement.pdf**.

*Acknowledgements.* This work was funded in part by NOAA's Health of the Atmosphere Program.

Edited by: N. M. Donahue

## References

Atkinson, R., Baulch, D. L., Cox, R. A., Crowley, J. N., Hampson, R. F., Hynes, R. G., Jenkin, M. E., Rossi, M. J., Troe, J., and IUPAC Subcommittee: Evaluated kinetic and photochemical data for atmospheric chemistry: Volume II – gas phase reactions of organic species, Atmos. Chem. Phys., 6, 3625–4055, doi:10.5194/acp-6-3625-2006, 2006.

Baasandorj, M., Papanastasiou, D. K., Talukdar, R. K., Hasson, A. S., and Burkholder, J. B.: $(CH_3)_3COOH$ (tert-butyl hydroperoxide): OH reaction rate coefficients between 206 and 375 K and the OH photolysis quantum yield at 248 nm, Phys. Chem. Chem. Phys., 12, 12101–12111, doi:10.1039/c0cp00463d, 2010.

Baeza-Romero, M. T., Glowacki, D. R., Blitz, M. A., Heard, D. E., Pilling, M. J., Rickard, A. R., and Seakins, P. W.: A combined experimental and theoretical study of the reaction between methylglyoxal and OH/OD radical: OH regeneration, Phys. Chem. Chem. Phys., 9, 4114–4128, 2007.

Barnes, I., Bastian, V., Becker, K. H., and Tong, Z.: Kinetics and products of the reactions of $NO_3$ with monoalkenes, dialkene and monoterpenes, J. Phys. Chem., 94, 2413–2419, 1990.

Boyd, A. A., Canosa-Mas, C. E., King, A. D., Wayne, R. P., and Wilson, M. R.: Use of a stopped-flow technique to measure the rate constants at room temperature for reactions between the nitrate radical and various organic species, J. Chem. Soc., Faraday Trans., 87, 2913–2919, 1991.

Canosa-Mas, C., Smith, S. J., Toby, S., and Wayne, R. P.: Temperature dependences of the reactions of the nitrate radical with some alkynes and with ethylene, J. Chem. Soc. Faraday Trans., 2, 263–272, 1988.

Chen, Y., Wang, W., and Zhu, L.: Wavelength-dependent photolysis of methylglyoxal in the 290–440 nm region, J. Phys. Chem. A, 104, 11126–11131, 2000.

D'Anna, B., Bakken, V., Beukes, J. A., Nielsen, C. J., Brudnik, K., and Jodkowski, J. T.: Experimental and theoretical studies of gas phase $NO_3$ and OH radical reactions with formaldehyde, acetaldehyde and their isotopomers, Phys. Chem. Chem. Phys., 5, 1790–1805, 2003.

Dlugokencky, E. J. and Howard, C. J.: Studies of $NO_3$ radical reactions with some atmospheric organic compounds at low pressures, J. Phys. Chem., 93, 1091–1096, 1989.

Ervens, B. and Volkamer, R.: Glyoxal processing by aerosol multiphase chemistry: towards a kinetic modeling framework of secondary organic aerosol formation in aqueous particles, Atmos. Chem. Phys., 10, 8219–8244, doi:10.5194/acp-10-8219-2010, 2010.

Espinosa-Garcia, J., Marquez, A., and Dobe, S.: Theoretical enthalpy of formation of the acetonyl radical, Chem. Phys. Lett., 373, 350–356, doi:10.1016/s0009-2614(03)00551-7, 2003.

Feierabend, K. J., Zhu, L., Talukdar, R. K., and Burkholder, J. B.: Rate coefficients for the OH+HC(O)C(O)H (glyoxal) ceaction between 210 and 390, J. Phys. Chem. A, 112, 73–82, 2008.

Feierabend, K. J., Flad, J. E., Brown, S. S., and Burkholder, J. B.: HCO quantum yields in the photolysis of HC(O)C(O)H (glyoxal) between 290 and 420 nm, J. Phys. Chem. A, 113, 7784–7794, 2009.

Fu, T.-M., Daniel J. Jacob, Wittrock, F., Burrows, J. P., Vrekoussis, M., and Henze, D. K.: Global budgets of atmospheric glyoxal and methylglyoxal, and implications for formation of secondary organic aerosols, J. Geophys. Res.-Atmos., 113, D15303, doi:10.1029/2007JD009505, 2008.

Galano, A., Alvarez-Idaboy, J. R., Ruiz-Santoyo, M. E., and Vivier-Bunge, A.: Mechanism and kinetics of the reaction of OH radicals with glyoxal and methylglyoxal: a quantum chemistry + CVT/SCT approach, Chem. Phys. Chem., 5, 1379–1388, doi:10.1002/cphc.200400127, 2004.

Goldstein, A. H. and Galbally, I. E.: Known and unexplored organic constituents in the earth's atmosphere, Environ. Sci. Technol., 41, 1514–1521, doi:10.1021/es072476p, 2007.

Green, M., Yarwood, G., and Niki, H.: FTIR study of the Cl-atom initiated oxidation of methylglyoxal, Int. J. Chem. Kinet., 22, 689–699, 1990.

Grossmann, D., Moortgat, G. K., Kibler, M., Schlomski, S., Bachmann, K., Alicke, B., Geyer, A., Platt, U., Hammer, M. U., Vogel, B., Mihelcic, D., Hofzumahaus, A., Holland, F., and Volz-Thomas, A.: Hydrogen peroxide, organic peroxides, carbonyl compounds, and organic acids measured at Pabsthum during BERLIOZ, J. Geophys. Res.-Atmos., 108, 8250, doi:10.1029/2001jd001096, 2003.

Hallquist, M., Wenger, J. C., Baltensperger, U., Rudich, Y., Simpson, D., Claeys, M., Dommen, J., Donahue, N. M., George, C., Goldstein, A. H., Hamilton, J. F., Herrmann, H., Hoffmann, T., Iinuma, Y., Jang, M., Jenkin, M. E., Jimenez, J. L., Kiendler-Scharr, A., Maenhaut, W., McFiggans, G., Mentel, Th. F., Monod, A., Prévôt, A. S. H., Seinfeld, J. H., Surratt, J. D., Szmigielski, R., and Wildt, J.: The formation, properties and impact of secondary organic aerosol: current and emerging issues, Atmos. Chem. Phys., 9, 5155–5236, doi:10.5194/acp-9-5155-2009, 2009.

Ho, K. F., Lee, S. C., Cao, J. J., Kawamura, K., Watanabe, T., Cheng, Y., and Chow, J. C.: Dicarboxylic acids, ketocarboxylic acids and dicarbonyls in the urban road-

side area of Hong Kong, Atmos. Environ., 40, 3030–3040, doi:10.1016/j.atmosenv.2005.11.069, 2006.

Jang, M. S. and Kamens, R. M.: Atmospheric secondary aerosol formation by heterogeneous reactions of aldehydes in the presence of a sulfuric acid aerosol catalyst, Environ. Sci. Technol., 35, 4758–4766, doi:10.1021/es010790s, 2001.

Jang, M. S., Carroll, B., Chandramouli, B., and Kamens, R. M.: Particle growth by acid-catalyzed heterogeneous reactions of organic carbonyls on preexisting aerosols, Environ. Sci. Technol., 37, 3828–3837, doi:10.1021/es021005u, 2003.

Jang, M. S., Czoschke, N. M., and Northcross, A. L.: Semiempirical model for organic aerosol growth by acid-catalyzed heterogeneous reactions of organic carbonyls, Environ. Sci. Technol., 39, 164–174, doi:10.1021/es048977h, 2005.

Karl, T., Harley, P., Emmons, L., Thornton, B., Guenther, A., Basu, C., Turnipseed, A., and Jardine, K.: Efficient Atmospheric Cleansing of Oxidized Organic Trace Gases by Vegetation, Science, 330, 816–819, doi:10.1126/science.1192534, 2010.

Kleindienst, T. E., Harris, G. W., and Pitts, J.: Rates and temperature dependences of the reaction of OH with isoprene, its oxidation products, and selected terpenes, Environ. Sci. Technol., 16, 844–846, 1982.

Kroll, J. H., Ng, N. L., Murphy, S. M., Varutbangkul, V., Flagan, R. C., and Seinfeld, J. H.: Chamber studies of secondary organic aerosol growth by reactive uptake of simple carbonyl compounds, J. Geophys. Res.-Atmos., 110, D23207, doi:10.1029/2005jd006004, 2005.

Liggio, J. and McLaren, R.: An optimized method for the determination of volatile and semi-volatile aldehydes and ketones in ambient particulate matter, Int. J. Environ. Anal. Chem., 83, 819–835, 2003.

Moortgat, G. K., Grossmann, D., Boddenberg, A., Dallmann, G., Ligon, A. P., Turner, W. V., Gab, S., Slemr, F., Wieprecht, W., Acker, K., Kibler, M., Schlomski, S., and Bachmann, K.: Hydrogen peroxide, organic peroxides and higher carbonyl compounds determined during the BERLIOZ campaign, J. Atmos. Chem., 42, 443–463, 2002.

Myriokefalitakis, S., Vrekoussis, M., Tsigaridis, K., Wittrock, F., Richter, A., Brühl, C., Volkamer, R., Burrows, J. P., and Kanakidou, M.: The influence of natural and anthropogenic secondary sources on the glyoxal global distribution, Atmos. Chem. Phys., 8, 4965–4981, doi:10.5194/acp-8-4965-2008, 2008.

Papadimitriou, V. C., Talukdar, R. K., Portmann, R. W., Ravishankara, A. R., and Burkholder, J. B.: $CF_3CF{=}CH_2$ and (Z)-$CF_3CF{=}CHF$: temperature dependent OH rate coefficients and global warming potentials, Phys. Chem. Chem. Phys., 10, 808–820, doi:10.1039/b714382f, 2008.

Papadimitriou, V. C., Lazarou, Y. G., Talukdar, R. K., and Burkholder, J. B.: Atmospheric chemistry of $CF_3CF{=}CH_2$ and (Z)-$CF_3CF{=}CHF$: Cl and $NO_3$ rate coefficients, Cl reaction product yields, and thermochemical calculations, J. Phys. Chem. A, 115, 167–181, doi:10.1021/jp110021u, 2011.

Paulot, F., Crounse, J. D., Kjaergaard, H. G., Kroll, J. H., Seinfeld, J. H., and Wennberg, P. O.: Isoprene photooxidation: new insights into the production of acids and organic nitrates, Atmos. Chem. Phys., 9, 1479–1501, doi:10.5194/acp-9-1479-2009, 2009.

Paulson, S. E. and Seinfeld, J. H.: Development and evaluation of a photooxidation mechanism for isoprene, J. Geophys. Res.-Atmos., 97, 20703–20715, 1992.

Plum, C. N., Sanhueza, E., akinson, R., Carter, W. P. L., and James, N. Pitts, J.: OH radical rate constants and photolysis rates of $\alpha$-dicarbonyls, Environ. Sci. Technol, 17, 479–484, 1983.

Profeta, L. T. M., Sams, R. L., Johnson, T. J., and Williams, S. D.: Quantitative Infrared Intensity Studies of Vapor-Phase Glyoxal, Methylglyoxal, and 2,3-Butanedione (Diacetyl) with Vibrational Assignments, J. Phys. Chem. A, 115, 9886–9900, doi:10.1021/jp204532x, 2011.

Rudich, Y., Talukdar, R. K., Fox, R. W., and Ravishankara, A. R.: Rate coefficients for reactions of $NO_3$ with a few olefins and oxygenated olefins, J. Phys. Chem., 100, 5374–5381, 1996.

Sander, S. P., Friedl, R. R., Golden, D. M., Huie, R. E., Kolb, C. E., Kurylo, M. J., Molina, M. J., Moortgat, G. K., Orkin, V. L., Ravishankara, A. R., and Finlayson-Pitts, B. J.: Chemical kinetics and photochemical data for use in atmospheric studies, JPL Pub. 10-6, Evaluation Number 17, Jet Propulsion Laboratory, Pasadena, 2011.

Smith, I. W. M. and Ravishankara, A. R.: Role of hydrogen-bonded intermediates in the bimolecular reactions of the hydroxyl radical, J. Phys. Chem. A, 106, 4798–4807, 2002.

Staffelbach, T. A., Orlando, J. J., Tyndall, G. S., and Calvert, J. G.: The UV-visible absorption-spectrum and photolysis quantum yields of methylglyoxal, J. Geophys. Res.-Atmos., 100, 14189–14198, 1995.

Talukdar, R. K., Burkholder, J. B., Schmoltner, A. M., Roberts, J. M., Wilson, R. R., and Ravishankara, A. R.: Investigation of the loss processes for peroxyacetyl nitrate in the atmosphere – UV photolysis and reaction with OH, J. Geophys. Res.-Atmos., 100, 14163–14173, 1995.

Talukdar, R. K., Gierczak, T., McCabe, D. C., and Ravishankara, A. R.: Reaction of hydroxyl radical with acetone. 2. Products and reaction mechanism, J. Phys. Chem. A, 107, 5021–5032, 2003.

Talukdar, R. K., Davis, M. E., Zhu, L., Ravishankara, A. R., and Burkholder, J. B.: Determination of the OH Radical Yield in the $CH_3CO + O_2 + M$ Reaction, 19th International Symposium on Gas Kinetics, 22–27 July 2006, Orleans, France, 2006.

Taylor, S. E., Goddard, A., Blitz, M. A., Cleary, P. A., and Heard, D. E.: Pulsed Laval nozzle study of the kinetics of OH with unsaturated hydrocarbons at very low temperatures, Phys. Chem. Chem. Phys., 10, 422–437, doi:10.1039/b711411g, 2008.

Tuazon, E. C. and Atkinson, R.: A product study of the gas-phase reaction of methyl vinyl ketone with the OH radical in the presence of $NO_x$, Int. J. Chem. Kinet., 21, 1141–1152, 1989.

Tyndall, G. S., Staffelbach, T. A., Orlando, J. J., and Calvert, J. G.: Rate coefficients for the reactions of OH radicals with methylglyoxal and acetaldehyde, Int. J. Chem. Kinet., 27, 1009–1020, 1995.

Vaghjiani, G. L. and Ravishankara, A. R.: Kinetics and mechanism of OH reaction with $CH_3OOH$, J. Phys. Chem., 93, 1948–1959, 1989.

Volkamer, R., Spietz, P., Burrows, J., and Platt, U.: High-resolution absorption cross-section of glyoxal in the UV-vis and IR spectral ranges, J. Photochem. Photobiol., A, 172, 35–46, 2005.

Zhang, L. M., Moran, M. D., Makar, P. A., Brook, J. R., and Gong, S. L.: Modelling gaseous dry deposition in AURAMS: a unified regional air-quality modelling system, Atmos. Environ., 36, 537–560, doi:10.1016/s1352-2310(01)00447-2, 2002.

Zhao, J., Levitt, N. P., Zhang, R., and Chen, J.: Heterogeneous reactions of methylglyoxal in acidic media: implications for secondary organic aerosol formation, Environ. Sci. Technol., 40, 7682–7687, doi:10.1021/es060610k, 2006.

Zhu, L., Talukdar, R. K., Burkholder, J. B., and Ravishankara, A. R.: Rate coefficients for the OH + acetaldehyde ($CH_3CHO$) reaction between 204 and 373 K, Int. J. Chem. Kinet., 40, 635–646, doi:10.1002/kin.20346, 2008.